Electrochemistry Communications 111 (2020) 106625

Contents lists available at ScienceDirect

Electrochemistry Communications

journal homepage: www.elsevier.com/locate/elecom

The impact of bulk electrolysis cycling conditions on the perceived stability of redox active materials

Jeffrey A. Kowalski[a,b], Bertrand J. Neyhouse[a,b], Fikile R. Brushett[a,b,*]

[a] Joint Center for Energy Storage Research, Massachusetts Institute of Technology, Cambridge 02139, USA
[b] Department of Chemical Engineering, Massachusetts Institute of Technology, Cambridge, MA 02139, USA

A B S T R A C T

Emerging grid storage needs are motivating the discovery and development of new, potentially inexpensive redox couples for use in flow batteries. Long-term stability in electrochemical environments remains a key challenge and charge/discharge cycling in a bulk electrolysis cell is a common initial approach. However, as cycling protocols are not yet standardized, comparison between different materials is difficult. Here, using a well-studied, substituted dialkoxybenzene as a model compound, we examine the impact of cycling conditions on perceived stability. Specifically, we show that cycle time is a better measure of stability than cycle number and, for materials that are unstable in their charged state, the fractional capacity accessed is inversely related to cycle time until failure.

1. Introduction

Redox flow batteries (RFBs) are a promising electrochemical technology for energy-intensive grid storage applications, but further cost reductions are needed for widespread adoption [1–3]. Expanding the redox chemistry design space beyond transition metal salts dissolved in aqueous acidic electrolytes may enable lower battery system costs through either reduced chemical costs or increased energy density [4,5]. Notably, the recent emergence and rapid advancement of redox active organic molecules in both aqueous and nonaqueous electrolytes offers intriguing new pathways to low cost energy storage through targeted molecular functionalization and inexpensive synthesis routes [6–8]. However, stability in the complex environments within operating electrochemical devices remains a key challenge for many of these new materials and, at present, lifetime projections fall short of what is thought necessary for commercial viability [7,9]. Continued progress requires the development of methods to rigorously characterize decay rates and elucidate decomposition mechanisms with the ultimate goal of informing design strategies for future materials. While analytical protocols are being established for a range of spectroscopic techniques (*e.g.*, EPR [10–12], NMR [13,14], UV–Vis [15,16]), the most common approach remains repetitive charge/discharge cycling in an electrochemical cell [9,14,15,17–19]. Typically, these studies are performed at dilute active species concentrations in a bulk electrolysis cell [14,17–19], but recently, more advanced symmetric flow cell cycling approaches have been developed for evaluating active species at higher concentrations [9,15]. Here we limit our focus to the former method, which remains more prevalent as it is easier and cheaper to set up and operate in a diverse set of laboratories, uses commercially available hardware, and requires less material.

At present, bulk electrolysis cycling protocols are not standardized and, consequently, a wide range of charging methods (*e.g.,* galvanostatic [14,20] and potentiostatic [9]), charging/discharging rates [14,15,17,21,22], state-of-charge (SOC) swings [15,17,18,20], cell geometries [14,17–19], and active species concentrations [14,15,17,21,22] are used. These inconsistencies challenge meaningful comparisons between newly-reported redox species because the experimental conditions can have a significant impact on the number of cycles until failure and, consequently, the perceived stability (or instability) of a material. In an effort to understand how cycling parameters can influence observed cycling performance of redox materials, we examine the impact of different charge/discharge rates and SOCs accessed using a commercial bulk electrolysis cell and a well-studied, moderately stable, substituted dialkoxybenzene, 2,5-di-*tert*-butyl-1,4-bis(2-methoxyethoxy)benzene (DBBB), dissolved in a nonaqueous electrolyte [18,20,23–26].

2. Material and methods

All work was completed inside of an argon-filled glovebox (MBraun Labmaster) with the water < 5 ppm and oxygen < 1 ppm at 26 °C (ambient glovebox temperature). Solutions were prepared using volumetric flasks and then diluted to the desired active species concentration. The electrolyte was 1 M lithium bis(trifluoromethanesulfonyl)-imide (LiTFSI, BASF, > 99.9% purity) in propylene carbonate (PC, BASF, > 99.9% purity), which were both used as received. DBBB was

* Corresponding author at: Department of Chemical Engineering, Massachusetts Institute of Technology, Cambridge, MA 02139, USA.
E-mail address: brushett@mit.edu (F.R. Brushett).

https://doi.org/10.1016/j.elecom.2019.106625
Received 26 September 2019; Received in revised form 21 November 2019; Accepted 29 November 2019
Available online 09 December 2019
1388-2481/

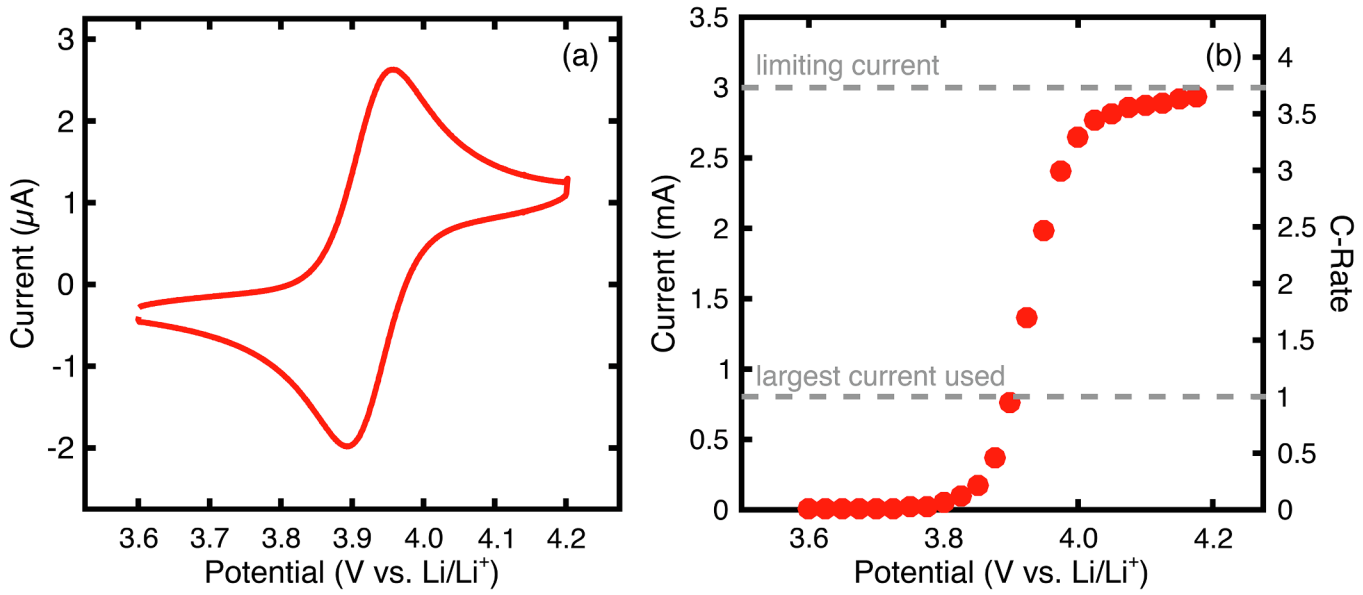

Fig. 1. Cyclic voltammogram of 0.001 M DBBB in 1 M LiTFSI in PC (a). Polarization curve for the bulk electrolysis cell using 0.001 M DBBB at 0% SOC in 1 M LiTFSI in PC showing the limiting current of about 3 mA (b). The C-rate on the second y-axis corresponds to the experimental set up of 0.001 M active material in 30 mL of solution with a stir rate of 1400 rpm.

synthesized and characterized as previously described [18,20,25]. This electrolyte composition was selected because of its large electrochemical stability window, moderate ionic conductivity, low volatility, and previously demonstrated compatibility with DBBB [20]. The active species concentration was always diluted to 0.001 M DBBB.

Electrochemical data was collected using a VSP-300 potentiostat (Bio-Logic). Before all bulk electrolysis experiments, cyclic voltammetry (Fig. 1a) was performed on the electrolyte solution to determine the higher and lower potential bounds for the cycling experiments, which were set to be *ca.* 0.3 V above and below the measured redox potential. Cyclic voltammetry measurements were performed in a three electrode cell with a 3 mm glassy carbon working electrode (CH Instruments, Inc.), a lithium foil (Alfa Aesar) counter electrode, and a fritted lithium foil (Alfa Aesar, fill solution: 1 M LiTFSI in PC) reference electrode at a scan rate of 20 mV s^{-1}. Before each voltammogram, the glassy carbon working electrode was polished on a MicroCloth pad with a slurry of 0.05 μm alumina powder (Buehler Ltd.) in deionized water (Millipore), rinsed with deionized water, and wiped dry with lens paper (VWR).

All cycling experiments were performed in a commercial bulk electrolysis cell (BASi, MF-1056) with 30 mL of solution containing electrolyte and active species. The working, counter, and reference electrodes were high surface area reticulated vitreous carbon (BASi, MF-2077), lithium foil (Alfa Aesar) in a fritted glass chamber (BASi, MR-1196), and fritted lithium foil (Alfa Aesar, fill solution: 1 M LiTFSI in PC), respectively. During operation, the solution was stirred at a rate of 1400 rpm. Two different electrochemical experiments were performed: sample-current polarization to determine the limiting current of the cell and extended galvanostatic charge/discharge cycling to determine cycle stability. For the polarization experiments, the electrode potential was stepped from 3.6 V to 4.175 V vs. Li/Li^+ in increments of 0.025 V and holds of 2 min, which was sufficient to reach a steady state current. Between each potential step, the electrode voltage was lowered to 3.6 V vs. Li/Li^+ for 10 min to reduce any oxidized species and return the solution to 0% SOC. Extended cycling was performed using a galvanostatic method with the same current for both charging and discharging. The applied currents were 0.804 mA, 0.402 mA, 0.201 mA, and 0.1005 mA, which correspond to 1C, 0.5C, 0.25C, and 0.125C, respectively. When attempting to access 100% SOC, only potential limits were set as determined from the cyclic voltammograms; whereas when attempting to access 50% SOC, both time and potential cutoffs were applied. The potential cutoffs were set to *ca.* 0.3 V above and below the redox potential and the time cutoff was set to half of the initial theoretical capacity (*e.g.*, 1 h for 0.5C). Whichever cutoff was reached first determined the end of the half cycle. Each independent charging/discharging rate and SOC accessed was performed in duplicate using two different cells with separately prepared electrolyte solutions. Note for all presented cycle data, the different cells are shown on independent plots to improve the clarity except when comparing the two cells directly. For each cycle, both the time and accessed capacity varies for the different cells used.

3. Results and discussion

Prior to cycling experiments, the limiting current for the bulk electrolysis cell was determined to set upper bounds on the charging/discharging rates that could be applied. For bulk electrolysis, the limiting current depends on the active species concentration and diffusivity, cell geometry, stir rate, and the electrochemical surface area of the electrode. Fig. 1a and Fig. 1b show a representative cyclic voltammogram and polarization curve for one of the two cells used, respectively. Note that the measured limiting current was similar for both cells and was *ca.* 3 mA or 3.7C when using 30 mL of solution, 0.001 M DBBB, and a stir rate of 1400 rpm. Thus, to ensure that mass transfer limitations did not significantly impact cycling data, the largest currents chosen were about 25% of the limiting current (*ca.* 1C).

For all of the currents used, the charging capacity fade is comparable for both cells, as shown in Fig. 2. As expected, as the current increases, the capacity accessed decreases due to the increased cell polarization, setting an upper limit on the accessible capacity which is less than the theoretical capacity. In all cycling experiments, the coulombic efficiency of the first cycle was lower than that of the subsequent cycles. Specifically, for 1C, 0.5C, 0.25C, and 0.125C, the first cycle coulombic efficiency was about 58.1 ± 0.6%, 70.7 ± 0.2%, 70 ± 2%, and 66 ± 4%, respectively, while the average of the subsequent cycles was around 97.5 ± 0.4% (376 cycles using 2 cells), 94 ± 1% (143 cycles using 2 cells), 88 ± 2% (70 cycles using 2 cells), and 70 ± 5% (31 cycles using 2 cells), respectively. The low coulombic efficiencies of the first cycle are consistent with previous studies and are tentatively attributed to a combination of cell conditioning and the formation of a

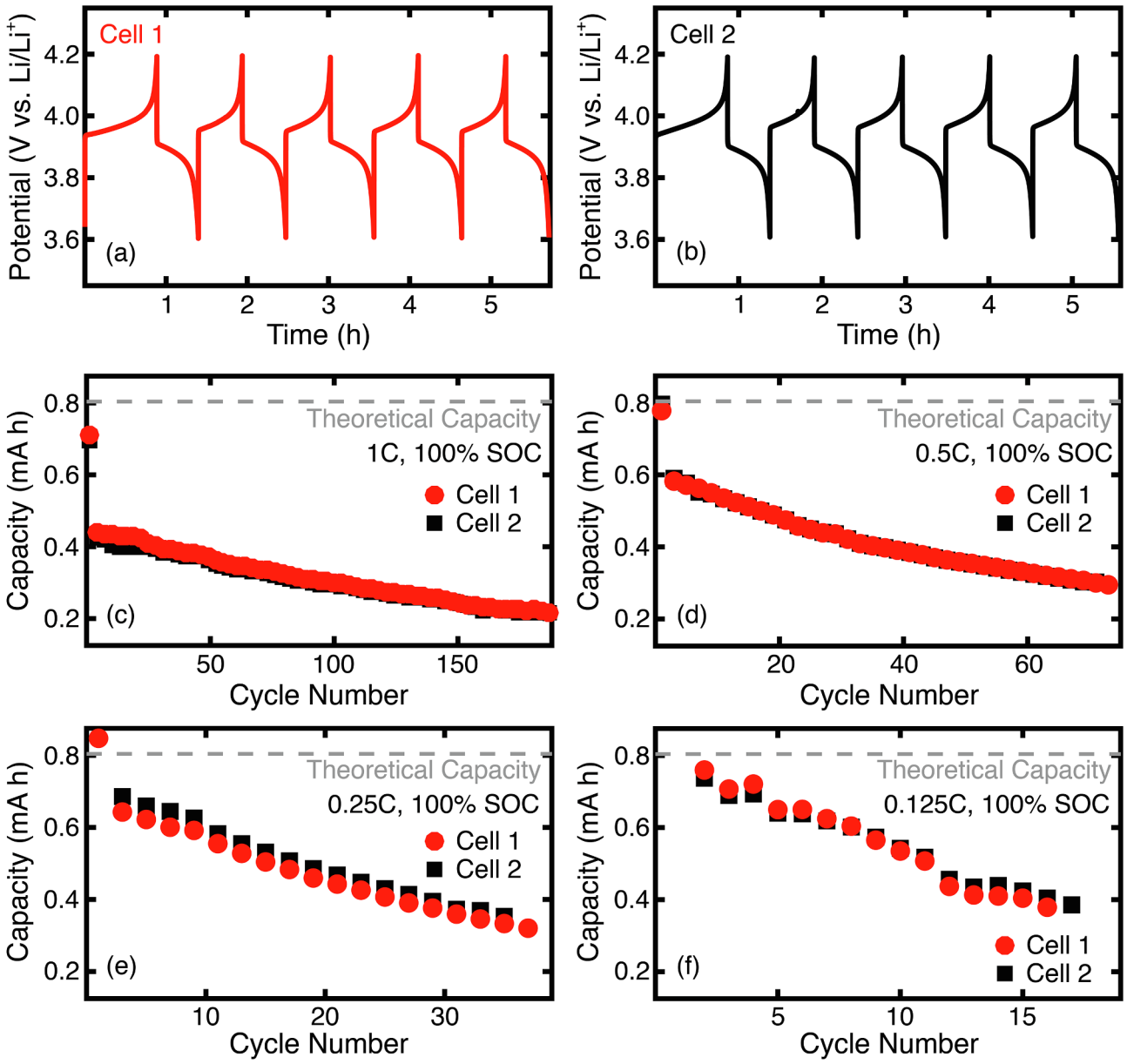

Fig. 2. First 5 bulk electrolysis cycles of 0.001 M DBBB in 1 M LiTFSI in PC in cell 1 (a) and cell 2 (b) with a charging/discharging rate of 1C accessing 100% SOC, and the charging capacity as a function of cycle number for each of the cells at a charging/discharging rate of 1C (0.804 mA, c), 0.5C (0.402 mA, d), 0.25C (0.201 mA, e), and 0.125C (0.1005 mA, f) while accessing 100% SOC.

solid electrolyte interphase on the lithium counter electrode [27,28]. Overall, the coulombic inefficiency is greater than the observed capacity fade rate, indicating that it is not completely due to irreversible capacity loss but, rather, is likely a result of species crossover to the counter electrode chamber in concert with an array of reversible and irreversible decay processes (*e.g.*, self-discharge, molecular decomposition). For example, in the case of 1C, the rate of capacity fade per cycle would be about 2.5% if the coulombic inefficiency led to an irreversible capacity loss; however, in reality, the fade rate is only 0.3% per cycle.

To determine the impact of charging rate, the capacity fade was evaluated as a function of cycle number, Fig. 3a and c, and cycling time, Fig. 3b and d. The charging capacity is normalized to the second cycle in order to more easily compare the rates of capacity fade by excluding the cell conditioning (first cycle) and minimizing the differences in accessed capacity due to the different applied currents.

To date, the most typical metric reported is the number of cycles before a set amount of capacity fade (Fig. 3a, c) [9,14,17–20,22,29]. While meaningful when comparing materials under identical conditions, variations in charging rate and accessed capacity convolute analysis. To illustrate this point, we first evaluate DBBB at different charging rates (1C, 0.5C, 0.25C, and 0.125C) but with similar nominal accessed capacities (100%). When comparing capacity fade per cycle, the DBBB stability appears to vary: 0.3% per cycle (1C), 0.7% per cycle (0.5C), 1.5% per cycle (0.25C), and 3.7% per cycle (0.125C). For example, at 1C, DBBB cycled for 186 cycles before the capacity dropped to 50% of the second cycle, whereas at 0.125C, the capacity dropped by 50% after only 16 cycles. In contrast, normalizing the capacity fade by time (Fig. 3b, d) appears a more accurate representation of stability. From Fig. 3, the cycling fade rate as a function of time is consistent across all charging rates used, 0.33 ± 0.04% per hour, 0.34 ± 0.01% per hour, 0.34 ± 0.01% per hour, and 0.37 ± 0.04% per hour for 1C, 0.5C, 0.25C, and 0.125C, respectively.

Next, to highlight another common inconsistency, we vary SOC

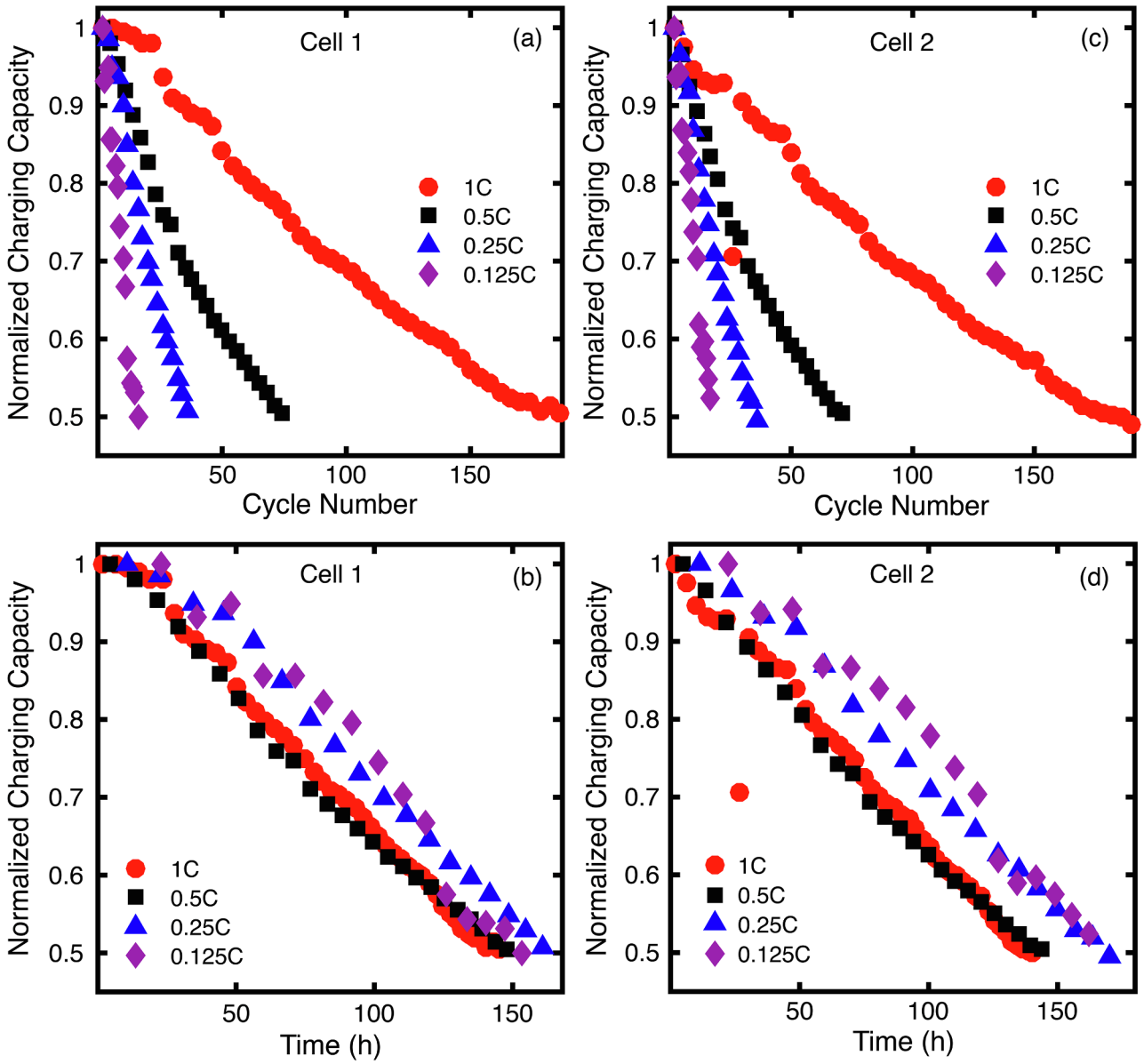

Fig. 3. Normalized charging capacity as a function of cycle number for cell 1 (a) and cell 2 (c) and time for cell 1 (b) and cell 2 (d) accessing 100% SOC for 1C (0.804 mA, red circles), 0.5C (0.402 mA, black squares), 0.25C (0.201 mA, blue triangles), and 0.125C (0.1005 mA, purple diamonds). The electrolyte used was 0.001 M DBBB in 1 M LiTFSI in PC. The charging capacity is normalized to the second charging cycle.

accessed by either cycling from 0% to 100% SOC or from 0% to 50% SOC [14,17,18,22]. The impact of the SOC range on the stability is shown in Fig. 4 using a C-rate of 0.5C (0.402 mA). Again, both the charging capacity fade as a function of cycle number (Fig. 4a, c) and cycling time (Fig. 4b, d) are shown.

As the same charging rate is shown, when comparing the cycle number and the cycle time, the data appears qualitatively similar; however, comparing different charging rates and SOCs accessed yields larger variations in the analyses (*e.g.*, comparing Figs. 4a to 3a). For the comparison of SOC accessed, the cycling time and cycle number are *ca.* 1.7× greater for the 50% SOC to achieve the same capacity fade as the 100% SOC. This is a consequence of it taking about 2× as long to decay below 0.40 mAh for 50% SOC for about 2/3 of the faded capacity, but the rate of decay from 0.40 mAh to 0.30 mAh is similar for both SOCs for about 1/3 of the capacity fade. Note, when charging to 100% SOC, only 0.59 mAh, 73% of the theoretical capacity (0.80 mAh), was accessed due to a combination of mass transport limitations, as evidenced by Fig. 1, and instability in the charged state, as described in Fig. 3. While at 50% SOC, 0.40 mAh was accessed, which is half of the theoretical capacity but 68% of the accessible capacity. Thus, in general, when accessing a lower fraction of the SOC, more cycles can be reached because, for each cycle, the active material is in the less stable, charged state for shorter times and at lower concentrations.

4. Conclusions

Though standardized testing protocols have yet to be agreed upon, the most common method of determining active materials stability is extended bulk electrolysis cycling until failure. However, variations in experimental conditions (*i.e.*, charge/discharge current, accessed capacity) can convolute results, challenging material comparisons across the published literature. In agreement with recent observations in symmetric flow cells, we find that the cycling time rather than cycle number is a better representation of stability as relevant chemical decomposition reactions are time-dependent [9,30]. In addition, we find that accessed capacity per cycle also impacts observed stability, due to

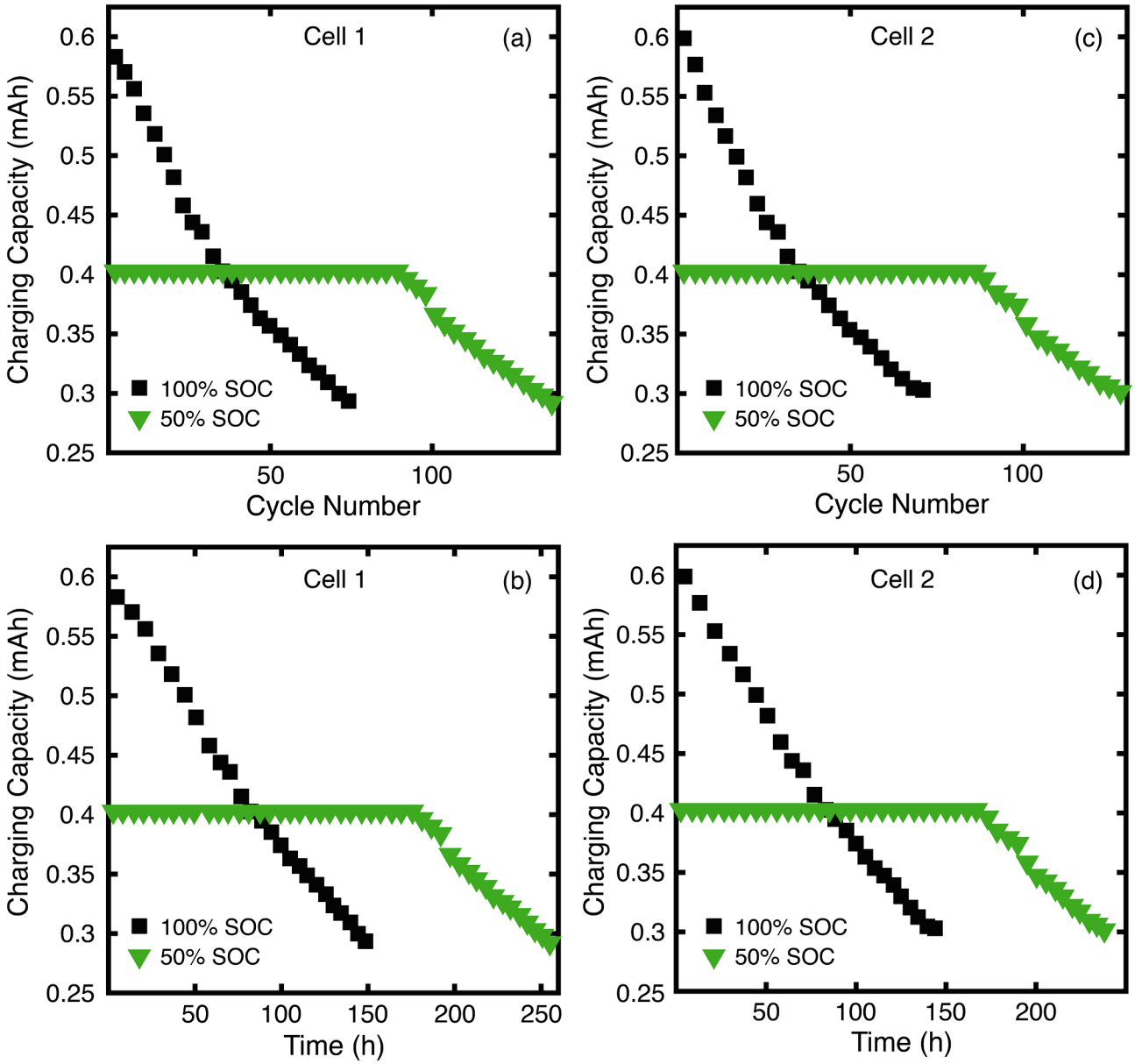

Fig. 4. Charging capacity as a function of cycle number for cell 1 (a) and cell 2 (c) and time for cell 1 (b) and cell 2 (d) accessing 100% SOC (black squares) and 50% SOC (green triangles) with a charging rate of 0.5C (0.402 mA). The electrolyte used was 0.001 M DBBB in 1 M LiTFSI in PC.

the time- and concentration-dependence of decomposition processes. As such, the important parameters for bulk electrolysis cycling appear to be how long the unstable species is present in solution and how concentrated the unstable species is in solution, which agrees with recent reports on species stability [9,30]. Other factors to be aware of in bulk electrolysis cycling are the cell limitations due to the geometry, supplied convection, and charging method. This includes how long the cell can be operated until crossover interferes with the results (especially for symmetric cell cycling), knowledge of the limiting current of the cell, and use of a charging/discharging rate that is application appropriate.

CRediT authorship contribution statement

Jeffrey A. Kowalski: Conceptualization, Methodology, Investigation, Validation, Data curation, Visualization, Writing - original draft, Writing - review & editing. **Bertrand J. Neyhouse:** Visualization, Writing - original draft, Writing - review & editing. **Fikile R. Brushett:** Conceptualization, Project administration, Supervision, Writing - original draft, Writing - review & editing.

Declaration of Competing Interest

The authors declare that they have no known competing financial interests or personal relationships that could have appeared to influence the work reported in this paper.

Acknowledgements

This work was supported as part of the Joint Center for Energy Storage Research, an Energy Innovation Hub funded by the U.S. Department of Energy, Office of Science, Basic Energy Sciences.

References

[1] A.Z. Weber, et al., J. Appl. Electrochem. 41 (2011) 1137–1164.
[2] L. Su, J.A. Kowalski, K.J. Carroll, F.R. Brushett, Rechargeable Batteries, Green Energy and Technology, Springer International Publishing, 2015, pp. 673–712.
[3] P. Alotto, M. Guarnieri, F. Moro, Renew. Sustain. Energy Rev. 29 (2014) 325–335.
[4] M.L. Perry, A.Z. Weber, J. Electrochem. Soc. 163 (2016) A5064–A5067.
[5] R.M. Darling, K.G. Gallagher, J.A. Kowalski, S. Ha, F.R. Brushett, Energy Environ.

Sci. 7 (2014) 3459–3477.
[6] J.A. Kowalski, L. Su, J.D. Milshtein, F.R. Brushett, Curr. Opin. Chem. Eng. 13 (2016) 45–52.
[7] C.G. Armstrong, K.E. Toghill, Electrochem. Commun. 91 (2018) 19–24.
[8] P. Leung, et al., J. Power Sources 360 (2017) 243–283.
[9] M.-A. Goulet, M.J. Aziz, J. Electrochem. Soc. 165 (2018) A1466–A1477.
[10] J. Zhang, et al., J. Phys. Chem. C 122 (2018) 8116–8127.
[11] J. Huang, et al., Sci. Rep. 6 (2016) 32102.
[12] J. Zhang, et al., Adv. Energy Mater. 7 (2017) 1701272.
[13] C.S. Sevov, et al., J. Am. Chem. Soc. 137 (2015) 14465–14472.
[14] C.S. Sevov, et al., J. Am. Chem. Soc. 139 (2017) 2924–2927.
[15] J.D. Milshtein, et al., Energy Environ. Sci. 9 (2016) 3531–3543.
[16] A.P. Kaur, N.E. Holubowitch, S. Ergun, C.F. Elliott, S.A. Odom, Energy Technol. 3 (2015) 476–480.
[17] J.A. Kowalski, et al., J. Mater. Chem. A 5 (2017) 24371–24379.
[18] J. Huang, et al., Adv. Energy Mater. 5 (2015) 1401782.
[19] S.M. Laramie, J.D. Milshtein, T.M. Breault, F.R. Brushett, L.T. Thompson, J. Power Sources 327 (2016) 681–692.
[20] J. Huang, et al., J. Mater. Chem. A 3 (2015) 14971–14976.
[21] T.J. Carney, S.J. Collins, J.S. Moore, F.R. Brushett, Chem. Mater. 29 (2017) 4801–4810.
[22] W. Duan, et al., ACS Energy Lett. 2 (2017) 1156–1161.
[23] F.R. Brushett, J.T. Vaughey, A.N. Jansen, Adv. Energy Mater. 2 (2012) 1390–1396.
[24] J. Zhang, et al., J. Phys. Chem. C 122 (2018) 8159–8172.
[25] L. Zhang, Z. Zhang, P.C. Redfern, L.A. Curtiss, K. Amine, Energy Environ. Sci. 5 (2012) 8204–8207.
[26] J. Zhang, et al., J. Phys. Chem. C 121 (2017) 23347–23358.
[27] M.B. Pinson, M.Z. Bazant, J. Electrochem. Soc. 160 (2013) A243–A250.
[28] W. Xu, et al., Energy Environ. Sci. 7 (2014) 513–537.
[29] X. Wei, et al., Adv. Mater. 26 (2014) 7649–7653.
[30] J. Zhang, J. Huang, L.A. Robertson, I.A. Shkrob, L. Zhang, J. Power Sources 397 (2018) 214–222.